

Ground and space signatures of VLF noise suppression by whistlers

David R. Shklyar¹, Jyrki Manninen², Elena E Titova³, Ondrej Santolík⁴, Ivana Kolmašová⁵, and Tauno Turunen⁶

¹Space Research Institute

²Sodankyla Geophysical Observatory

³Polar Geophysical Institute

⁴Department of Space Physics, Institute of Atmospheric Physics, The Czech Academy of Sciences, Prague, Czech Republic

⁵Department of Space Physics, Institute of Atmospheric Physics, The Czech Academy of Sciences

⁶Sodankylä Geophysical Observatory

November 24, 2022

Abstract

VLF spectrograms registered at Kannuslehto ground station, after cleaning them from strong sferics, reveal VLF noise suppression by whistlers and whistler echo trains, which consists in significant reduction in the noise spectral power after a strong whistler event. We have found similar effect in the VLF data from Van Allen Probe B taken in the equatorial region on L-shell ~ 3 . Detailed analysis of the data shows that the whistler echo train as well as the VLF noise have small wave normal angles. Based on this observation, we limit our analysis to parallel (ducted) whistler wave propagation. The persistence of whistler echo train as well as the VLF noise suggests that in the events under discussion, plasma is unstable in the frequency range corresponding to the observed VLF noise band. In an attempt to explain the effect of VLF noise suppression, we follow up the long-standing idea that relates this effect to the reduction of free energy in the unstable plasma distribution by whistler echo train. To develop this idea into qualitative model, we have studied the motion of energetic electrons, responsible for the noise generation, in the field of ducted whistler echo train. We show that energetic electrons that make the main contribution to the growth rate of VLF noise, during their bounce oscillations in the magnetosphere are subject to multiple resonant impacts from the whistler echo train. These lead to energetic electron diffusion in the phase space, and the corresponding reduction in free energy of the unstable distribution.

Ground and space signatures of VLF noise suppression by whistlers

D. R. Shklyar,^{1,2} J. Manninen,³ E. E. Titova,^{4,1} O. Santolík,^{5,6} I. Kolmašová,^{5,6}
and T. Turunen³

¹Space Research Institute, Russian Academy of Sciences, Moscow, Russia.

²National Research University Higher School of Economics, Moscow, Russia.

³Sodankylä Geophysical Observatory, Sodankylä, Finland.

⁴Polar Geophysical Institute, Apatity, Russia.

⁵Department of Space Physics, Institute of Atmospheric Physics, Czech Academy of Sciences, Prague, Czechia.

⁶Faculty of Mathematics and Physics, Charles University, Prague, Czechia.

Key Points:

- Masked VLF wave phenomena are revealed by “cleaning” from sferics spectrograms registered at Kannuslehto ground station.
- VLF noise suppression by strong whistlers is due to whistler related modification of electron distribution in the noise generation region.
- This modification is caused by phase space diffusion of energetic electrons in the field of multihop whistler.

Corresponding author: J. Manninen, Jyrki.Manninen@sgo.fi

Abstract

VLF spectrograms registered at Kannuslehto ground station, after cleaning them from strong sferics, reveal VLF noise suppression by whistlers and whistler echo trains, which consists in significant reduction in the noise spectral power after a strong whistler event. We have found similar effect in the VLF data from Van Allen Probe B taken in the equatorial region on L -shell ~ 3 . Detailed analysis of the data shows that the whistler echo train as well as the VLF noise have small wave normal angles. Based on this observation, we limit our analysis to parallel (ducted) whistler wave propagation. The persistence of whistler echo train as well as the VLF noise suggests that in the events under discussion, plasma is unstable in the frequency range corresponding to the observed VLF noise band. In an attempt to explain the effect of VLF noise suppression, we follow up the long-standing idea that relates this effect to the reduction of free energy in the unstable plasma distribution by whistler echo train. To develop this idea into qualitative model, we have studied the motion of energetic electrons, responsible for the noise generation, in the field of ducted whistler echo train. We show that energetic electrons that make the main contribution to the growth rate of VLF noise, during their bounce oscillations in the magnetosphere are subject to multiple resonant impacts from the whistler echo train. These lead to energetic electron diffusion in the phase space, and the corresponding reduction in free energy of the unstable distribution.

1 Introduction

In this paper we discuss the wave phenomenon in VLF frequency band which consists in transient reduction in the amplitude of VLF noise observed, first on the ground, after receiving a strong whistler. An example of this phenomenon is shown in Figure 1, which displays the spectrogram in the frequency band up to 8 kHz registered at Kannuslehto ground station in Finland on 25 December 2011. The upper panel shows the wave magnetic field power spectral density over a 4 minute interval. A significant decrease in spectral amplitude of VLF noise after receiving a strong whistler is clearly visible. We will turn our attention to other panels of Figure 1 later on. Other examples of VLF noise suppression by strong whistler echo trains, registered at Kannuslehto ground station, may be found in the supplementary material to the paper.

Suppression effect under discussion was known for a long time. Based on observations on Siple Station, *Helliwell et al.* [1980] reported one-to-one correlation between hiss and optical emission ($\lambda 4278$) intensity reductions immediately following each discrete VLF event.

50 Since optical emission was assumed to result from particle precipitation, the authors suggested
51 that both the hiss and optical emission reductions were caused by pitch angle scattering of en-
52 ergetic electrons by whistlers.

53 A comprehensive study of whistler induced suppression of VLF noise has been performed
54 by *Gail and Carpenter* [1984]. The authors have established several important features of the
55 suppression effect, in particular, they demonstrated that the effect usually occurs when the driv-
56 ing whistler exhibits echoes confined to the frequency band occupied by the suppressed noise.
57 They have also shown that the recovery of the noise band to the pre-event level takes several
58 seconds, and this time correlates with the damping rate of the echo train. The effect of sup-
59 pression of the VLF noise band produced by the whistler that triggered it has been reported
60 by *Platino et al.* [2005] basing on observations by the Cluster spacecraft.

61 The explanation of the noise suppression suggested by *Helliwell et al.* [1980] and ac-
62 cepted by *Gail and Carpenter* [1984] consists in pitch angle scattering of energetic electrons
63 by the whistler signal that leads to disruption of wave amplification in the magnetospheric in-
64 teraction region. Those electrons which are scattered into the loss cone are observed as pre-
65 cipitation, providing the correlation between $\lambda 4278$ optical emission and VLF noise suppres-
66 sion. We should mention that, although the pitch angle scattering may lead to reduction in the
67 particle pitch angle anisotropy and, thus, decrease the amplification efficiency, the electrons
68 close to the loss cone do not contribute significantly to the noise amplification due to small
69 amplitude of interaction between these particles and parallel propagating whistler waves.

70 **2 Experimental features of suppression phenomenon**

71 **2.1 Ground based observations**

72 Let us return to Figure 1 which presents the observations of VLF noise suppression by
73 whistlers performed at Kannuslehto ground station (KAN) in Finland (67.74N, 26.27E; $L =$
74 5.5) on 25 December 2011. As was mention above, the upper panel displays the power spec-
75 tral density of the wave magnetic field and illustrates the phenomenon under discussion. This
76 spectrogram was preliminary cleaned from sferics using the method described in *Manninen*
77 *et al.* [2016]. Pay attention that a pronounced decrease in the noise intensity is observed af-
78 ter the second dispersed trace of the whistler echo train. Only the frequency band up to 8 kHz
79 is displayed, although VLF emissions were recorded in the frequency range from 0.2 to 39
80 kHz. Magnetic field measurements were performed using two mutually orthogonal magnetic

81 loop antennas oriented in the geographical north-south and east-west directions. This allows
82 us to determine the polarization of waves which is characterized by the parameter p :

$$p = 10 \cdot \log_{10} \left(\frac{|H_R|^2}{|H_L|^2} \right), \quad (1)$$

83 where $H_{R,L} = (H_N \pm iH_E)/\sqrt{2}$ are the right- and left-hand polarized horizontal magnetic field
84 components, respectively, and $H_{N,E}$ are the northward and eastward projections of the wave mag-
85 netic field. This parameter, displayed in the middle panel of Figure 1, shows that both whistlers
86 and VLF noise have left-hand polarization, which indicates that the signals come to the Kan-
87 nuslehto station over the Earth-ionosphere waveguide [*Ostapenko et al.*, 2010]. The lower panel
88 of Figure 1 displays the angle (with an ambiguity of 180°) between the minor axis of the wave
89 polarization ellipse and the north-south direction, which determines (with the same ambigu-
90 ity) the direction of wave arrival at the station. Close values of the displayed quantity for both
91 whistlers and noise suggest that they have close exit regions from the ionosphere. As for time
92 characteristics of the noise suppression phenomenon, it becomes the most pronounced about
93 15 – 30 seconds after strong whistler event and lasts several tens of seconds.

94 **2.2 Space observations onboard Van Allen Probes (RBSP)**

95 We have not found suppression events in Cluster or RBSP data simultaneous with any
96 one observed at Kannuslehto ground station. And an independent suppression event that we
97 have found in RBSP-B data, and which is discussed below, is quite weak.

98 Intense whistlers and echo trains were registered onboard RBSP-B on 22 December 2014.
99 VLF spectrogram up to 11 kHz obtained from electric (a) and magnetic (b) field measurements
100 of the EMFISIS instrument [*Kletzing et al.*, 2013] during the time period 19:23:29 - 19:24:23
101 UT when the instrument operated in the burst mode is shown in Figure 2. During this time
102 RBSP-B was in the morning sector in the southern hemisphere and had the following coor-
103 dinates: MLT ~ 5 h, MLAT $\sim -18^\circ$, and $L \sim 3$. Both electric and magnetic receivers reg-
104 istered whistlers, sometimes with their echoes, and VLF noise below 6 kHz. The most intense
105 whistlers were registered at about 19:24 UT, first a fractional-hop whistler at 19:23:57 UT, which
106 came from the southern hemisphere, and then three echo signals, after which a decrease in the
107 VLF noise intensity below 6 kHz can be observed. Minimum intensity of the VLF noise was
108 observed ~ 20 s after the first reflected whistler.

109 Suppression of the noise intensity by whistler can be clearly seen from Figure 3b which
110 shows electric field spectral density in three narrow frequency channels 3988, 5020, and 5623

111 Hz in the time interval 19:20 - 19:28 UT. Three distinct spikes of spectral amplitude, which
 112 we associate with multihop whistlers (marked by “w” in the figure), followed by decrease in
 113 the noise amplitude are clearly seen. Minimum values of the noise intensity marked by arrows
 114 are observed $\sim 15 - 30$ s after whistlers.

115 Figure 3a shows cold plasma density [Kurth *et al.*, 2015] along the satellite trajectory,
 116 which smoothly increases between 19:21 and 19:24 UT, then remains almost constant and then
 117 slightly decreases after 19:27:30 UT. The amplitudes of whistlers and VLF noise also increase
 118 till 19:24 UT, whereupon intense whistlers are not observed, while the amplitude of noise slowly
 119 decreases. Simultaneous increase of the cold plasma density and VLF wave amplitudes (both
 120 of whistlers and VLF noise) may be related to ducting of whistler waves by density gradient
 121 of the cold plasma [Inan and Bell, 1977; Semenova and Trakhtengerts, 1980].

122 Ducted propagation of whistlers and VLF noise is confirmed by multicomponent anal-
 123 ysis of VLF waves. Figure 4 shows (a) the sum of power spectral densities of three magnetic
 124 field components, (b) planarity of the wave magnetic field [Santolík *et al.*, 2002], (c) wave nor-
 125 mal angle [Santolík *et al.*, 2003], and (d) a spectral estimate of a polar angle of Poynting vec-
 126 tor with respect to the ambient magnetic field [Santolík *et al.*, 2010]. One can see that fractional-
 127 hop whistler propagates towards the northern hemisphere, while multihop whistlers propagate
 128 towards the southern hemisphere. VLF noise also propagates towards the southern hemisphere.
 129 An important result that follows from the multicomponent analysis consists in that both whistlers
 130 and VLF noise have small wave normal angles. This suggests that the observed multihop whistlers
 131 propagate in ducted mode, and that VLF noise is most probably generated at the equator.

132 To check the assumption that resonant interaction of energetic electrons with multihop
 133 whistlers changes their distribution in such a way that the free energy of the distribution is de-
 134 creased, leading to the corresponding decrease in the growth rate, we have calculated the growth
 135 rates for parallel propagating whistler waves using the data from MagEIS instrument on RBSP-
 136 B [Blake *et al.*, 2013]. This growth rate is determined by the expression given in Sagdeev and
 137 Shafranov [1961]. Assuming that electron distribution function determining the growth rate
 138 is the function of particle kinetic energy $w = mv^2/2$ and magnetic momentum $\mu = mv_{\perp}^2/2\omega_c$
 139 (m , v , v_{\perp} are electron mass, total and transverse velocities, respectively, and ω_c is electron
 140 cyclotron frequency) this expression takes the form:

$$\gamma_{\parallel} = \omega \frac{8\pi^3 e^2 \omega_c (\omega_c - \omega)}{m^2 k^3 c^2} \int_0^{\infty} d\mu f'_0(\mu) \mu. \quad (2)$$

141 Here ω is the wave angular frequency, k is the magnitude of the wave normal vector, e is the
 142 magnitude of electron charge, c is the speed of light, and

$$f'_0(\mu) = \left(\frac{\partial f_0}{\partial \mu} + \omega \frac{\partial f_0}{\partial w} \right)_{w=mv_R^2/2+\mu\omega_c}, \quad (3)$$

143 where

$$v_R = \frac{\omega - \omega_c}{k} \quad (4)$$

144 is the resonance velocity at the first cyclotron resonance, the only one that exists at parallel
 145 propagation. As it is indicated above, after taking the derivatives in (3), particle parallel ve-
 146 locity is equated to v_R , so that the combined derivative (3) becomes a function of the magnetic
 147 momentum.

148 Electron distribution function that enters the above relations is determined from the mea-
 149 sured electron differential flux by the relation [Cornilleau-Wehrin *et al.*, 1985]:

$$f(w, \mu) \simeq 1.67 \cdot 10^{-37} \frac{J}{W}. \quad (5)$$

Relation (5) determines the electron distribution function in CGS system of units, used in the
 paper, through the measured differential electron flux J expressed in practical units, i.e.,

$$(\text{cm}^{-2} \cdot \text{s}^{-1} \cdot \text{sr}^{-1} \cdot \text{keV}^{-1})$$

150 and the particle energy in keV denoted by W . We should underline that, no matter in which
 151 variables the distribution function is expressed, it is always equal to particle density in the phase
 152 space (\mathbf{r}, \mathbf{v}) .

153 Normalized growth rates calculated from RBSP-B data for various moments before and
 154 after strong whistler events are shown in Figures 5-6. We see that the decrease of growth rate
 155 after one whistler event is quite small, although the decrease of growth rate after the series of
 156 three multihop whistlers is significant. Qualitative explanation of this result follows from the
 157 consideration in the next section.

158 While the decrease in the growth rate related to strong whistler events is clearly seen
 159 in Figures 5-6, the unstable frequency band does not correspond to that of equatorial VLF noise.
 160 The reason for this is that those growth rates are local, calculated at the latitude $\sim -18.6^\circ$,
 161 but not at the equator where the VLF noise is supposed to be generated. At the latitude $\sim -18.6^\circ$
 162 the loss-cone is wider than at the equator, while the cyclotron frequency and, thus, the reso-
 163 nance velocity are larger. Due to these, outside the equator we should expect smaller values

164 of the growth rate, but wider unstable frequency range. This is confirmed by direct calcula-
 165 tion of the growth rate at the equator, at the same L -shell where the suppression phenomenon
 166 has been observed, but at other time. This growth rate is shown in Figure 7. We see that at
 167 the equator, the growth rate is one order of magnitude larger than outside the equator, and the
 168 frequency of the growth rate maximum corresponds much better to the observed frequency band
 169 of VLF noise.

170 **3 Qualitative model of the VLF noise suppression by whistlers**

171 **3.1 Main assumptions of the model**

172 A general idea, which has been put forward by *Helliwell et al.* [1980] and *Gail and Car-*
 173 *penter* [1984] for explanation of the wave phenomenon under discussion, consists in the mod-
 174 ification of the electron distribution function by whistler in the way that reduces plasma in-
 175 stability causing the hiss generation. In the present study we follow up this idea and develop
 176 it into a qualitative model. A few assumptions suggested by observations that we use are the
 177 following.

- 178 1. VLF noise is generated in the equatorial region of the magnetosphere by unstable plasma
 179 distribution, and is characterized by a quasi-parallel direction of the wave normal vec-
 180 tors.
- 181 2. Whistler echo train causing the noise suppression propagates in ducted mode and can
 182 be describe in the approximation of parallel propagation.
- 183 3. At the pre-event stage, the plasma is in a marginally unstable state, the upper frequency
 184 of the observed noise band corresponding to the boundary between unstable and sta-
 185 ble frequency bands.
- 186 4. In the magnetospheric region, where the strong whistler interactions with resonant elec-
 187 trons responsible for the noise generation takes place, the electromagnetic field of the
 188 whistler echo train can be represented as a sum of three wave packets with varying fre-
 189 quencies and wave numbers; the frequency range of the causative whistler echo train
 190 overlaps the frequency band occupied by the suppressed noise.
- 191 5. While the strong whistler changes the energetic particle distribution, the generation of
 192 VLF hiss may be described in linear approximation, i.e., neglecting the back influence
 193 of the noise upon resonant particle distribution.

194 3.2 Energetic electron motion in the field of whistler echo train

195 Since VLF noise suppression is usually observed after the second dispersed whistler trace,
 196 we will assume the wave field to consist of three wave packets: a fractional-hop whistler orig-
 197 inating from a lightning stroke in the southern hemisphere (for the sake of definiteness), and
 198 two reflected whistlers, one from the northern and one from the southern hemisphere. Based
 199 on experimental observations, we will assume parallel propagation of all waves, which essen-
 200 tially simplifies the problem. In the case of parallel propagation, the wave field has only x -
 201 and y -components, transverse to the direction of wave propagation. Thus, we will write the
 202 wave electric field in the form:

$$E_x(z, t) = - \sum_i E_{0i}(z, t) \cos \Psi_i(z, t) \quad E_y = \sum_i E_{0i}(z, t) \sin \Psi_i(z, t); \quad (i = 1, 2, 3), \quad (6)$$

203 where z is the coordinate along the ambient magnetic field, $E_{0i}(z, t)$, $\Psi_i(z, t)$ are amplitudes
 204 and phases of the i -th wave packet. In the following numerical calculations, we will not con-
 205 sider space-time variation of the wave amplitudes, but will put them equal to 8 mV/m wher-
 206 ever the wave packets exist. At the same time, we will use exact expressions for wave packet
 207 phases as they follow from the equations of geometrical optics.

208 The wave frequency and the wave normal vector in each wave packet are determined
 209 in the usual way:

$$\omega_i(z, t) = - \frac{\partial \Psi_i(z, t)}{\partial t} \quad k_{zi}(z, t) \equiv k_i(z, t) = \frac{\partial \Psi_i(z, t)}{\partial z}. \quad (7)$$

210 In each wave packet, the wave frequency $\omega_i(z, t)$ and the wave normal vector $k_i(z, t)$ depend
 211 on both coordinate z and time t , but for each z and t they are related by the dispersion rela-
 212 tion for parallel propagating whistler mode waves, namely:

$$\frac{k^2(z, t) c^2}{\omega^2(z, t)} = 1 + \frac{\omega_p^2(z)}{\omega(z, t)[\omega_c(z) - \omega(z, t)]}, \quad (8)$$

213 where $\omega(z, t)$ and $k(z, t)$ are the frequency and the wave number defined above which depend
 214 on (z, t) , $\omega_p(z)$ is electron plasma frequency that depends on z , $\omega_c(z)$ is, as before, the elec-
 215 tron cyclotron frequency which also depends on z . The wave frequency in each wave packet
 216 calculated from the equations of geometrical optics under assumption of parallel propagation
 217 is shown in Figure 8. For given frequency $\omega(z, t)$ and coordinate z , the wave number $k(z, t)$,
 218 up to its sign, is determined by (8). For the first and the third wave packets $k(z, t) > 0$, while
 219 for the second wave packet $k(z, t) < 0$.

220 In non-relativistic approximation, and for parallel propagating whistler-mode wave, the
 221 resonance between the wave and electron arises under condition $v_{\parallel} = (\omega - \omega_c)/k$. Corre-

222 spondingly, electron resonance parallel energy in keV, with the account of (8), is given by

$$w_{\parallel res}(z, t) \equiv \frac{m[\omega(z, t) - \omega_c(z)]^2}{2k^2(z, t)} \frac{1}{\text{keV}} \simeq 256 \cdot \frac{[\omega_c(z) - \omega(z, t)]^3}{\omega(z, t)\omega_p^2(z)}, \quad (9)$$

223 where $\text{keV} = 1.6 \cdot 10^{-9}$. The quantity $w_{\parallel res}(z, t)$ in space-time domains where the multi-
224 hop whistler exists is shown in Figure 9.

225 The wave electric field in the form (6) corresponds to right-hand polarization with re-
226 spect to the ambient magnetic field independently of the sign of wave number k , i.e., of the
227 direction of the wave propagation. In our case, k_1 and k_3 are positive, while k_2 is negative.
228 The wave magnetic field can be found from the wave electric field (6) using the Faraday in-
229 duction law.

230 In the absence of the wave field, particle kinetic energy w and magnetic momentum μ
231 are conserved, and the particle motion can be described by the equations that follow from the
232 unperturbed Hamiltonian

$$H_0 = \frac{p_{\parallel}^2}{2} + \mu\omega_c(z), \quad (10)$$

233 where canonically conjugated variables are (p_{\parallel}, z) and (μ, φ) , where φ is the particle gyrophase.
234 Transverse components of electron velocity are expressed in canonical variables as follows:

$$v_x = \sqrt{\frac{2\mu\omega_c(z)}{m}} \cos \varphi; \quad v_y = \sqrt{\frac{2\mu\omega_c(z)}{m}} \sin \varphi. \quad (11)$$

235 We now write the variation of electron kinetic energy due to interaction with the whistler
236 echo train:

$$\frac{dw}{dt} \equiv -e\mathbf{E}\mathbf{v} = e\sqrt{\frac{2\mu\omega_c(z)}{m}} \sum_i E_{0i} \cos[\Psi_i(z, t) + \varphi], \quad (12)$$

237 where $-e$ is electron charge. As has been shown by *Shklyar and Matsumoto* [2009], for res-
238 onant particles, the rate of energy variation coincides with partial derivative of the interaction
239 Hamiltonian with respect to time. Taking this into account, and making use of (10) we come
240 to the expression for the total Hamiltonian of the problem in the form

$$H = \frac{p_{\parallel}^2}{2} + \mu\omega_c(z) - e\sqrt{\frac{2\mu\omega_c(z)}{m}} \sum_i \frac{E_{0i}}{\omega_i(z, t)} \sin[\Psi_i(z, t) + \varphi]. \quad (13)$$

241 The equations of motion which follow from the Hamiltonian (13) have the form:

$$\begin{aligned} \frac{dz}{dt} &= \frac{p_{\parallel}}{m}; \quad \frac{dp_{\parallel}}{dt} = -\mu \frac{d\omega_c}{dz} + e\sqrt{\frac{2\mu\omega_c(z)}{m}} \sum_i \frac{E_{0i}k_i(z, t)}{\omega_i(z, t)} \cos[\Psi_i(z, t) + \varphi]; \\ \frac{d\varphi}{dt} &= \omega_c(z) - e\sqrt{\frac{\omega_c(z)}{2\mu m}} \sum_i \frac{E_{0i}}{\omega_i(z, t)} \sin[\Psi_i(z, t) + \varphi]; \quad \frac{d\mu}{dt} = e\sqrt{\frac{2\mu\omega_c(z)}{m}} \sum_i \frac{E_{0i}}{\omega_i(z, t)} \cos[\Psi_i(z, t) + \varphi], \end{aligned} \quad (14)$$

242 where we have neglected the derivatives with respect to z of slowly varying quantities $\omega_i(z, t)$, $k_i(z, t)$
 243 and E_{0i} in the interaction Hamiltonian.

244 In the set of equations (14), the quantity φ is an unknown function, while the quanti-
 245 ties $\Psi_i(z, t)$ should be considered as known ones. However, the equations of geometrical opti-
 246 cally from which the quantities $\Psi_i(z, t)$ should be found define first of all their derivatives, i.e.,
 247 the quantities $\omega_i(z, t)$ and $k_i(z, t)$. That is why, in the equations of motion (14), it is conve-
 248 nient to use quantities $\zeta_i = \Psi_i(z, t) + \varphi$ as new unknown functions, since the function φ
 249 enters the equations of motion only in combinations ζ_i . Thus, instead of equation for φ and
 250 equations for $\Psi_i(z, t)$ it is more convenient to use the equations for ζ_i , which follow from the
 251 definitions given above and the equation for φ :

$$\frac{d\zeta_i}{dt} = \frac{k_i(z, t)p_{\parallel}}{m} - \omega_i(z, t) + \omega_c(z) - e\sqrt{\frac{\omega_c(z)}{2\mu m}} \sum_i \frac{E_{0i}}{\omega_i(z, t)} \sin \zeta_i . \quad (15)$$

252 In these equations, the quantities $k_i(z, t)$ and $\omega_i(z, t)$ are the functions that are found directly
 253 from the equations of geometrical optics.

254 The solution of the set of equations (14) for one particle is shown in Figures 10-11. Up-
 255 per panels of Figure 10 show the variation of latitude and normalized parallel velocity along
 256 the particle trajectory. We see that, on large time scale, the particle bounce-oscillates between
 257 mirror points occasionally experiencing resonant impacts from the multihop whistler. These
 258 impacts change the particle energy and magnetic momentum, the variation taking place dur-
 259 ing a very short time as compared to bounce period. One of such impacts is zoomed in the
 260 bottom right panel of the figure. As one can see from Figures 11, which displays the varia-
 261 tion of particle magnetic momentum (upper panel), each impact corresponds to stationary phase
 262 point in one of the wave packets, i.e., to the moment at which one of the derivatives $d\zeta_i/dt$
 263 shown in three lower panels turns to zero. We suggest that random jumps of electron energy
 264 and magnetic momentum in the course of interaction with multihop whistlers cause particle
 265 diffusion in the phase space, which leads to a decrease in free energy of the unstable distri-
 266 bution and the corresponding decrease of the growth rate.

For quantitative estimation of the suggested mechanism, we have calculated the aver-
 age variation squared, during the duration of the whistler echo train $\Delta t = 2.24$ s, of mag-
 netic momentum for 100 particles with initial energy $w = 132$ keV and magnetic momen-
 tum such that $\mu\omega_{ceq} = 56.6$ keV, uniformly distributed over gyrophases and the accessible
 range of initial latitudes on $L = 3$. These determine the particle diffusion coefficient $D_{\mu\mu}$

according to the relation

$$D_{\mu\mu} = \frac{\overline{(\Delta\mu)^2}}{2\Delta t}.$$

For the parameters of the model described above, the calculations give

$$\frac{\overline{(\Delta\mu)^2}}{\mu^2} = 0.072,$$

267 so that $D_{\mu\mu}/\mu^2 \simeq 0.016 \text{ s}^{-1}$. This gives the characteristic diffusion time $t_D \simeq 31 \text{ s}$, which
 268 also provides an estimation for the relaxation time of unstable plasma distribution.

269 **4 Concluding remarks**

270 We have presented experimental evidences of VLF noise suppression by strong whistlers
 271 which is observed on VLF spectrograms obtained at Kannoslehto ground station, after clean-
 272 ing them from sferics, as well as on spectrograms obtained on the Van Allen Probe B satel-
 273 lite. The idea that we use to explain this phenomenon can be traced back to early works by
 274 *Helliwell et al.* [1980] and *Gail and Carpenter* [1984]. It consists in the assumption that, due
 275 to interaction with strong whistler, the unstable electron distribution is modified in such a way
 276 that decreases the instability threshold. This modification should first of all be revealed at the
 277 boundary of unstable band, as is indeed observed in experiment.

278 To develop these ideas, we set forth a theory of electron resonant interaction with par-
 279 allel propagating multihop whistlers. We have derived and solved numerically the set of equa-
 280 tions that describe electron motion in the field of three wave packets representing the multi-
 281 hop whistler, and the ambient inhomogeneous geomagnetic field. These equations take into
 282 account space-time variations of frequencies and wave vectors in the packets, as well as space-
 283 time boundedness of the wave packets. We have shown that resonant interaction with such wave
 284 packets leads to electron diffusion in the phase space. We suggest that this diffusion causes
 285 the modification of unstable electron distribution and is responsible for the suppression effect.

286 **Acknowledgments**

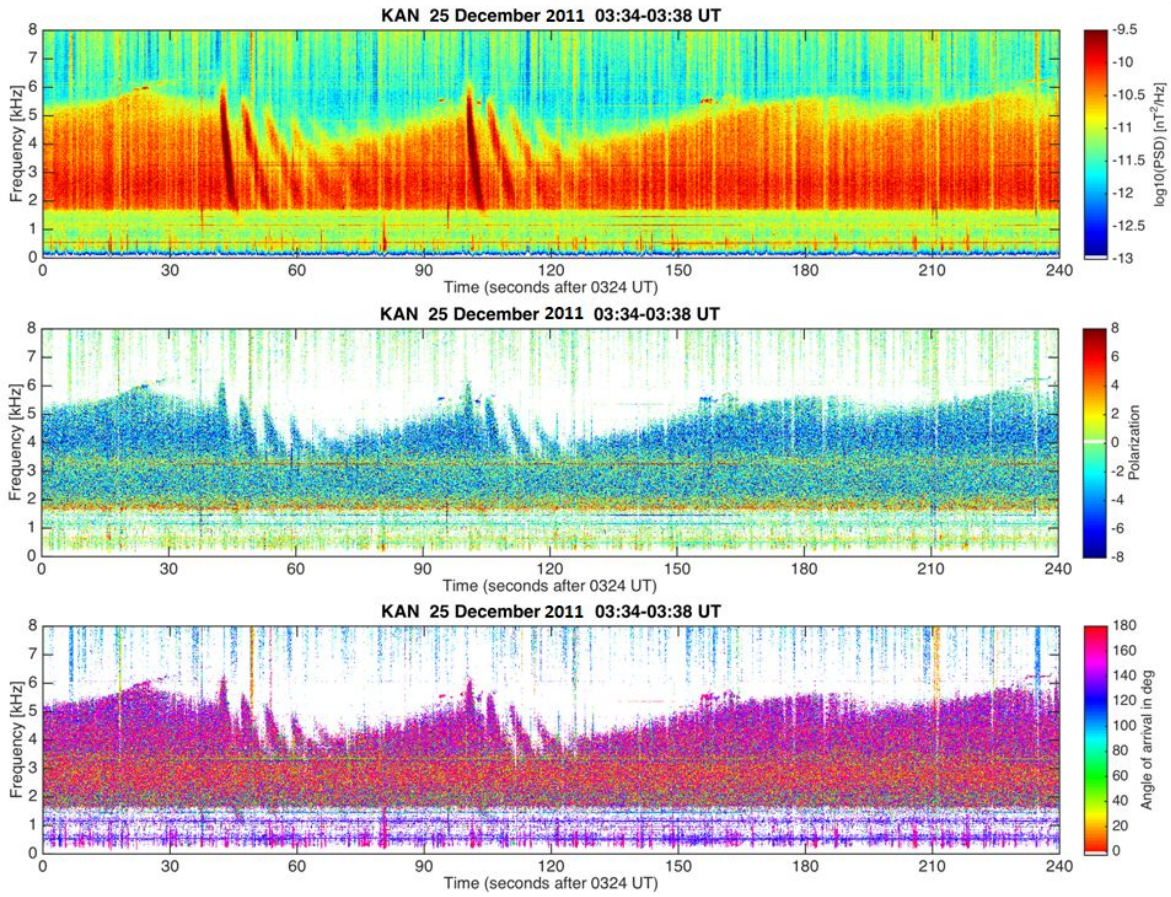
287 This study was done in the frame of the grant No. 294931 of the Academy of Sciences of Fin-
 288 land. D. R. S. and E. E. T. also acknowledge support from RFBR grant 19-02-00179. O.S.
 289 and I.K. acknowledge support from grants LTAUSA17070, GACR 17-07027S, and the Praemium
 290 Academiae award from the CAS. The authors thank the PI of EMFISIS instrument C. Klet-
 291 zing and the PI of MagEIS instrument H. Spence of Van Allen Probes team for the use of the

292 data which is available at http://cdaweb.sci.gsfc.nasa.gov/istp_public/. SGO ELF-VLF quick-
 293 look plots are available at http://www.sgo.fi/pub_vlf/.

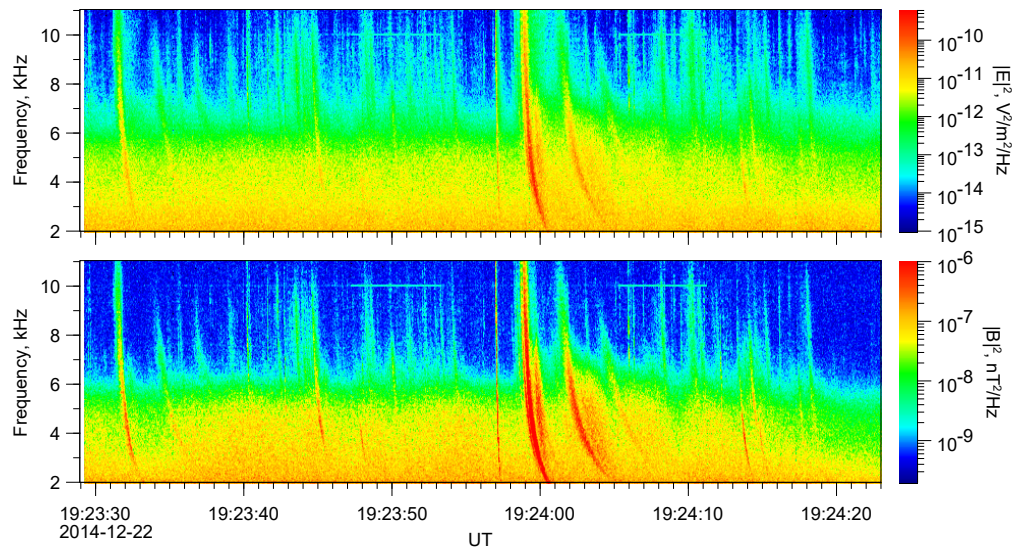
294 References

- 295 Blake, J. B. et al. (2013), The Magnetic Electron Ion Spectrometer (MagEIS) Instruments
 296 Aboard the Radiation Belt Storm Probes (RBSP) Spacecraft, *Space Science Reviews*,
 297 doi: 10.1007/s11214-013-9991-8.
- 298 C. A. Kletzing, W. S. Kurth, M. Acuna, R. J. MacDowall, R. B. Torbert, T. Averkamp,
 299 D. Bodet, S. R. Bounds, M. Chutter, J. Connerney, D. Crawford, J. Dolan, R. Dvorsky,
 300 G. Hospodarsky, J. Howard, V. Jordanova, R. Johnson, D. Kirchner, B. Mokrzycki, G.
 301 Needel, J. Odom, D. Mark, J. Phillips, C. Piker, S. Remington, O. Santolik, R. Schnurr,
 302 D. Sheppard, C. W. Smith, R. M. Thorne, & J. Tyler (2013), The Electric and Magnetic
 303 Field Instrument Suite and Integrated Science (EMFISIS) on RBSP, *Space Sci. Rev.*,
 304 179, 127–181, doi: 10.1007/s11214-013-9993-6.
- 305 Cornilleau-Wehrin, N, J. Solomon, A. Korth, & G. Kremser (1985), Experimental study
 306 of the relationship between energetic electrons and ELF waves observed on board
 307 GEOS: a support to quasi-linear theory, *J. Geophys. Res.*, 90, 4141–4154.
- 308 Gail, W. B., & D. L. Carpenter (1984), Whistler induced suppression of VLF noise, *J.*
 309 *Geophys. Res.*, 89(2), 1015–1022.
- 310 Helliwell, R. A., S. B. Mende, J. H. Doolittle, W. C. Armstrong, & D. L. Carpenter
 311 (1980), Correlations between $\lambda 4278$ optical emissions and VLF wave events observed at
 312 $L \sim 4$ in the Antarctic, *J. Geophys. Res.*, 85, 3376-3386.
- 313 Inan, U. S., & T. F. Bell (1977), The plasmopause as a VLF wave guide, *J. Geophys. Res.*,
 314 82(19), 2819-2827, doi:10.1029/JA082i019p02819.
- 315 Jyrki Manninen, Tauno Turunen, Natalia Kleimenova, Michael Rycroft, Liudmila Gro-
 316 mova, & Iina Sirviö (2016), Unusually high frequency natural VLF radio emis-
 317 sions observed during daytime in Northern Finland, *Environ. Res. Lett.*, 11, 124006,
 318 doi:10.1088/1748-9326/11/12/124006.
- 319 Kurth, W. S., S. De Pascuale, J. B. Faden, C. A. Kletzing, G. B. Hospodarsky, S. Thaller,
 320 & J. R. Wygant (2015), Electron densities inferred from plasma wave spectra obtained
 321 by the waves instrument on Van Allen Probes, *Journal of Geophysical Research: Space*
 322 *Physics*, 120, 904–914, <https://doi.org/10.1002/2014JA020857>.

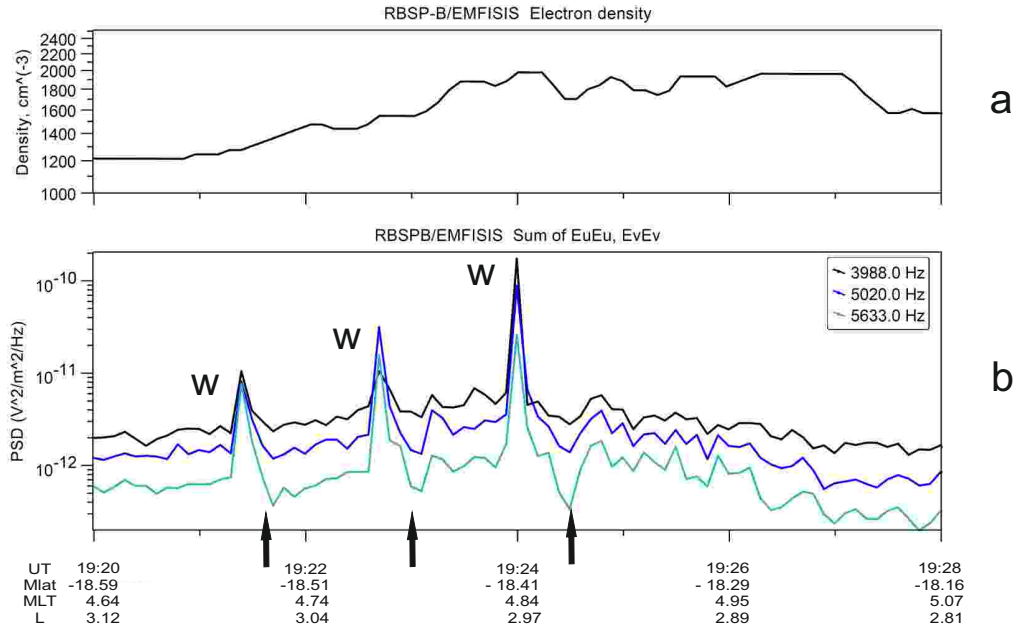
- 323 Ostapenko, A. A., E. E. Titova, A. P. Nickolaenko, T. Turunen, J. Manninen, & T. Raita
324 (2010), Characteristics of VLF atmospherics near the resonance frequency of the Earth-
325 ionosphere waveguide 1.62.3 kHz by observations in the auroral region, *Ann. Geophys.*,
326 28, 193-202.
- 327 Platino, M., U. S. Inan, T. F. Bell, D. A. Gurnett, J. S. Pickett, P. Canu, & P. M. E.
328 Décréau (2005), Whistlers observed by the Cluster spacecraft outside the plasmasphere,
329 *J. Geophys. Res.*, 110, A03212, doi:10.1029/2004JA010730.
- 330 Sagdeev, R. Z. and V. D. Shafranov (1961), On the instability of a plasma with an
331 anisotropic distribution of velocities in a magnetic field, *Sov. Phys. JETP*, 12, 130–132.
- 332 Santolk, O., J. S. Pickett, D. A. Gurnett, & L.R.O. Storey (2002), Magnetic component of
333 narrow-band ion cyclotron waves in the auroral zone, *J. Geophys. Res.*, 107(A12), 1444.
334 <https://doi.org/10.1029/2001JA000146>.
- 335 Santolk, O., Parrot, M., & Lefeuvre, F. (2003). Singular value decomposi-
336 tion methods for wave propagation analysis, *Radio Science*, 38(1), 1010.
337 <https://doi.org/10.1029/2000RS002523>.
- 338 Santolk, O., J. S. Pickett, D. A. Gurnett, J. D. Menietti, B. T. Tsurutani, & O. Verkho-
339 glyadova (2010), Survey of Poynting flux of whistler mode chorus in the outer zone, *J.*
340 *Geophys. Res.*, 115, A00F13. doi:10.1029/2009JA014925.
- 341 Semenova, V. I., & V. Yu. Trakhtengerts (1980), On specific features of the LF waveguide
342 propagation, *Geomagn. Aeron.*, 20(6), 1021-1027.
- 343 Shklyar, D., & H. Matsumoto (2009), Oblique whistler-mode waves in the inhomogeneous
344 magnetospheric plasma: Resonant interactions with energetic charged particles, *Surveys*
345 *in geophysics*, 30(2), 55–104.



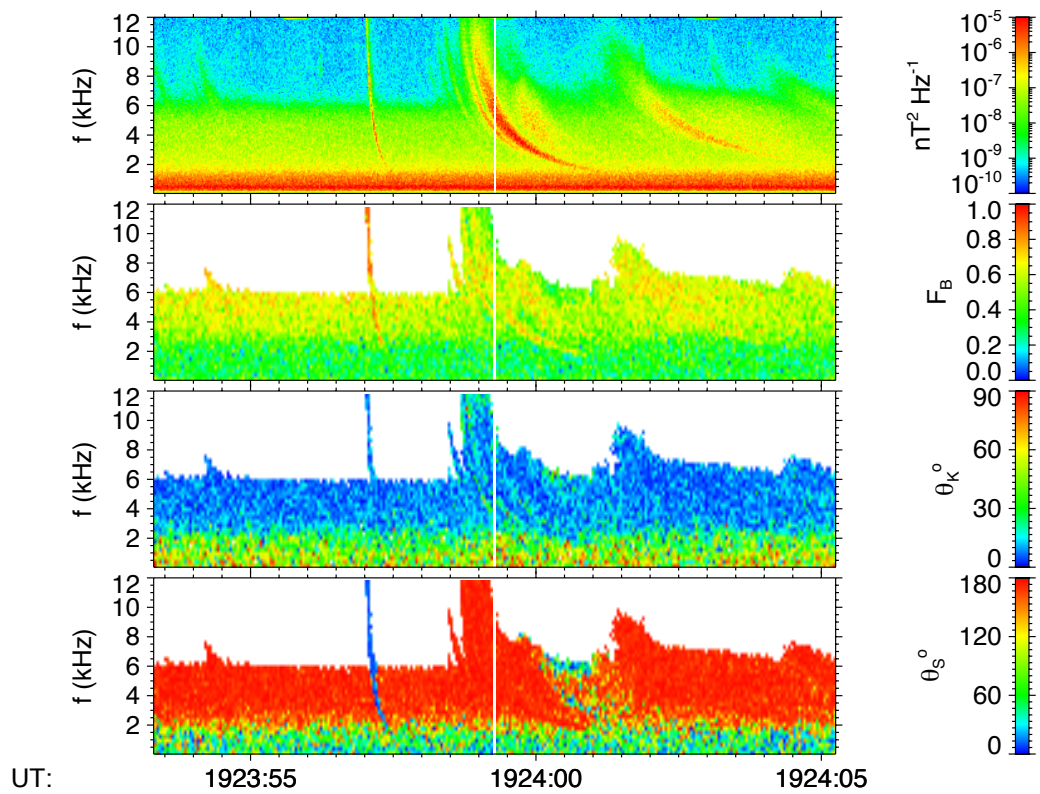
346 **Figure 1.** An example of spectrogram, obtained from ground station data, illustrating whistler induced
 347 suppression of VLF noise. (a) Logarithm of the total magnetic field power spectral density. (b) Parameter
 348 characterizing the wave polarization (see the text). (c) The angle between minor axis of the wave polarization
 349 ellipse and the north-south direction.



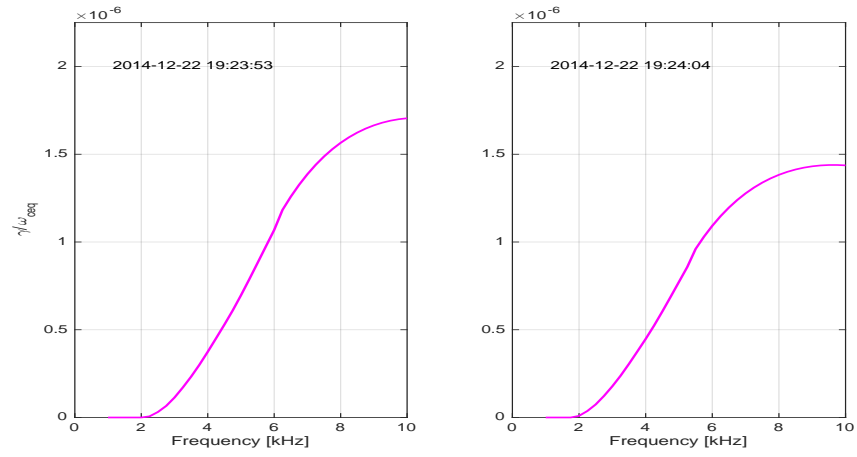
350 **Figure 2.** Dynamic spectra of VLF emission computed from RBSP-B waveform data for wave event ob-
351 served on 22 December 2014. The sum of the power spectral densities of three orthogonal (a) electric and (b)
352 magnetic components.



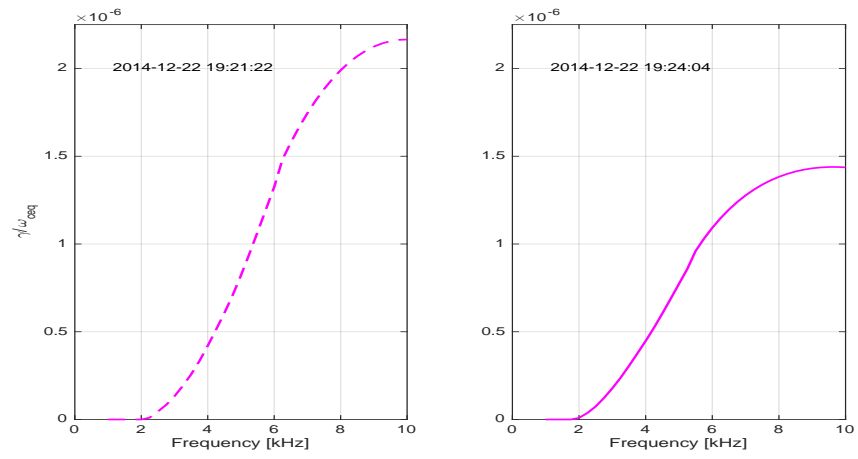
353 **Figure 3.** (a) Cold plasma density measured by RBSP-B. (b) Electric field spectral power of VLF emission
 354 detected in three frequency channels centered on 3988, 5020, and 5633 Hz.



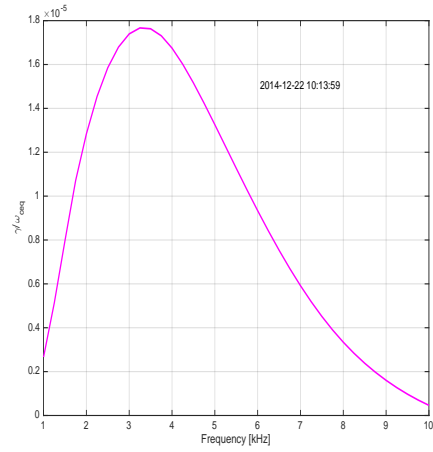
355 **Figure 4.** The results of multicomponent analysis of VLF wave measurements by RBSP-B on 22 December
 356 2014 (see text for explanation of the displayed quantities).



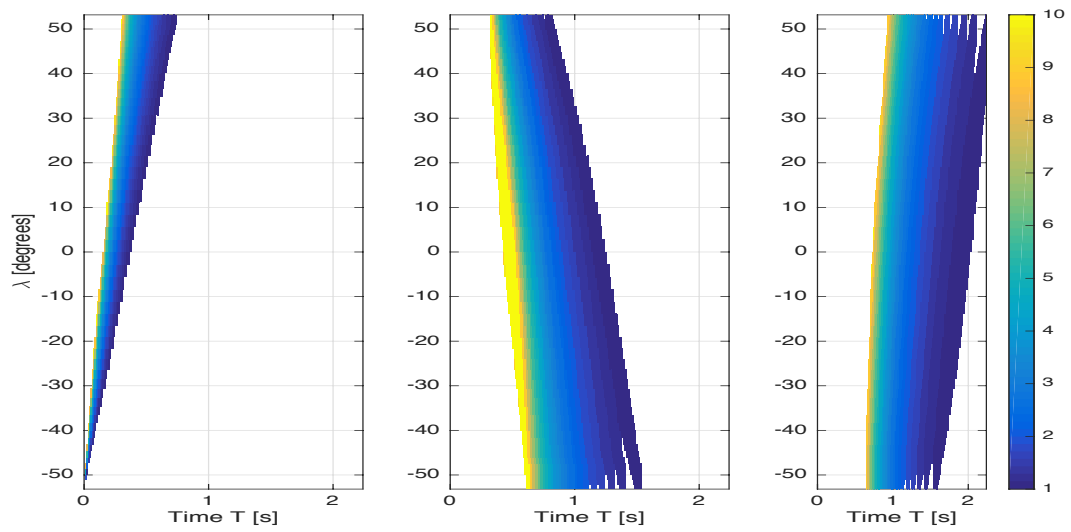
357 **Figure 5.** Growth rate as a function of frequency for parallel propagating whistler-mode waves calculated
 358 from RBSP-B measurements of electron fluxes by MagEIS instrument. Left and right panels display the
 359 normalized growth rate before and after the third whistler shown in Figure 3.



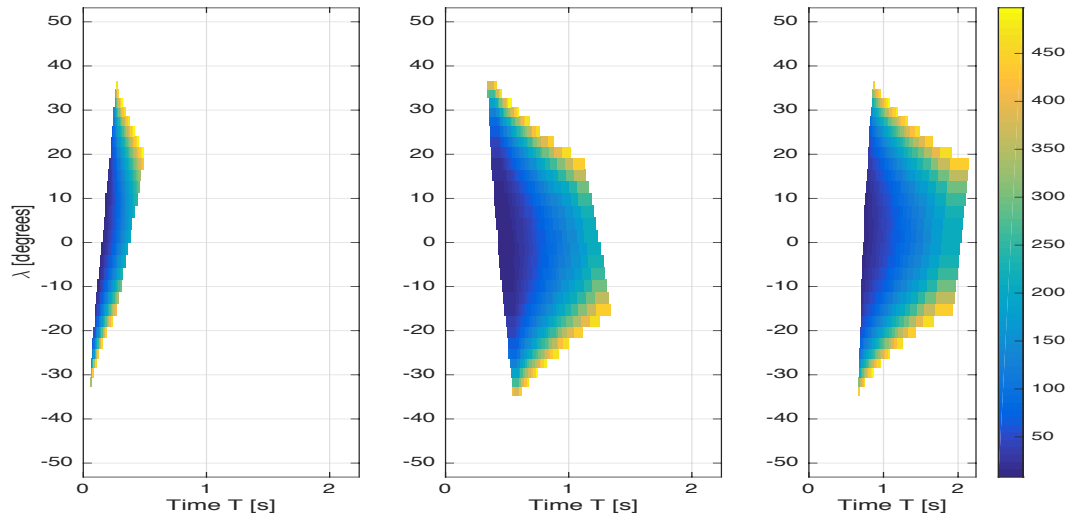
360 **Figure 6.** Just like above, but for moments before and after the series of whistlers shown in Figure 3.



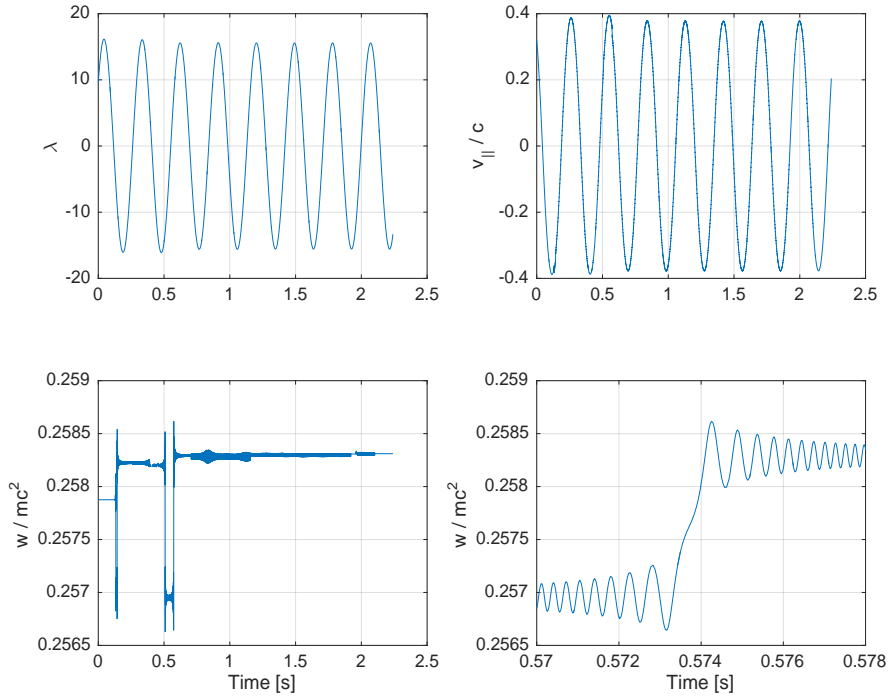
361 **Figure 7.** Growth rate at the equator ($L = 3.09$, $\lambda = 0.75^\circ$) as a function of frequency calculated from
362 electron fluxes measured by MagEIS instrument on RBSP-B on 22 December 2012, at 10:13:59 UT.



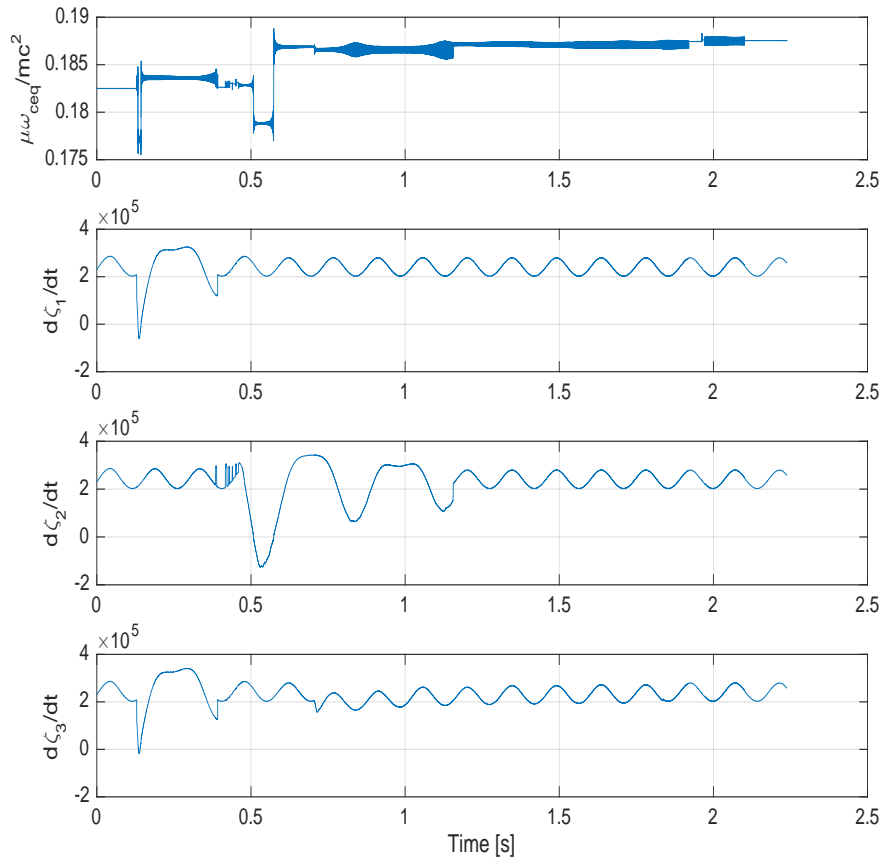
363 **Figure 8.** Frequency in kHz, colorcoded according to the colorbar, in space-time domain of three wave
364 packets corresponding to multihop whistler: (left) fractional-hop whistler, (middle) second-hop whistler re-
365 flected from the ground in the northern hemisphere, and (right) third-hop whistler reflected from the ground in
366 the southern hemisphere.



367 **Figure 9.** Resonance energy in keV, colorcoded according to colorbar, in space-time domain for three wave
 368 packets corresponding to multihop whistler (see the caption to Figure 8). Only domains where the resonance
 369 energy calculated according to non-relativistic expression is below 500 keV are displayed.



370 **Figure 10.** Time variations of particle latitude λ , longitudinal velocity v_{\parallel} , and kinetic energy w along the
 371 trajectory in the field of multihp whistler and the ambient geomagnetic field. Initial parameters of the particle
 372 are as follows: $\lambda_0 = 9.5865^\circ$; $v_{\parallel 0} = 0.32 c$; $\zeta_{1,0} = 6.0287 \text{ rad}$; $\mu_0 \omega_{ceq} = 0.1825 \text{ mc}^2$; $w_0 = 0.2579 \text{ mc}^2$.
 373 The particle moves along $L = 3$ where electron cyclotron frequency at the equator $\omega_{ceq} = 2.02 \cdot 10^5 \text{ rad}$.



374 **Figure 11.** Time variations of particle magnetic momentum and derivatives of the phases of three wave
 375 packets representing multihop whistler. Initial conditions are the same as in the Figure 10.